

Efficient molecular dynamics and hybrid Monte Carlo algorithms for path integrals

Cite as: J. Chem. Phys. **99**, 2796 (1993); <https://doi.org/10.1063/1.465188>

Submitted: 30 November 1992 • Accepted: 28 April 1993 • Published Online: 04 June 1998

Mark E. Tuckerman, Bruce J. Berne, Glenn J. Martyna, et al.



View Online



Export Citation

ARTICLES YOU MAY BE INTERESTED IN

[Efficient stochastic thermostating of path integral molecular dynamics](#)

The Journal of Chemical Physics **133**, 124104 (2010); <https://doi.org/10.1063/1.3489925>

[Quantum statistics and classical mechanics: Real time correlation functions from ring polymer molecular dynamics](#)

The Journal of Chemical Physics **121**, 3368 (2004); <https://doi.org/10.1063/1.1777575>

[Exploiting the isomorphism between quantum theory and classical statistical mechanics of polyatomic fluids](#)

The Journal of Chemical Physics **74**, 4078 (1981); <https://doi.org/10.1063/1.441588>

Lock-in Amplifiers
up to 600 MHz



Zurich
Instruments



Efficient molecular dynamics and hybrid Monte Carlo algorithms for path integrals

Mark E. Tuckerman^{a)} and Bruce J. Berne

Department of Chemistry, Columbia University, New York, New York 10027

Glenn J. Martyna and Michael L. Klein

Department of Chemistry, University of Pennsylvania, Philadelphia, Pennsylvania

(Received 30 November 1992; accepted 28 April 1993)

New path integral molecular dynamics (PIMD) and path integral hybrid Monte Carlo (PIHMC) algorithms are developed. It is shown that the use of a simple noncanonical change of variables that naturally divides the quadratic part of the action into long and short wavelength modes and multiple time scale integration techniques results in very efficient algorithms. The PIMD method also employs a constant temperature MD technique that has been shown to give canonical averages even for stiff systems. The new methods are applied to the simple quantum mechanical harmonic oscillator and to electron solvation in fluid helium and xenon. Comparisons are made with PIMC and the more basic PIMD and PIHMC methods.

I. INTRODUCTION

Monte Carlo (MC) and molecular dynamics (MD) methods are often used to evaluate discretized Euclidean time path integrals.¹⁻⁴ In their simplest forms, these methods converge slowly because the harmonic part of the action arising from the kinetic energy of the quantum particles is stiff. In MC, this permits only small moves of the "beads" representing the imaginary time slices.¹ In MD, this stiff part of the action leads to the use of small time steps. It also leads to nonergodic dynamics characteristic of the KAM regime where time averages are not equal to phase space averages.⁵ This second condition has generally been alleviated by employing periodic velocity refreshes.⁶ Efficient MC schemes overcome the difficulty caused by the stiff action through the use of a good choice of conditional probability distribution function within the Metropolis MC algorithm.² Two new and comparably efficient MD methods are developed in this paper. This is important because MD programs can be structured to achieve high performance on parallel, vector as well as simple serial computer architectures. In addition, MD schemes can straightforwardly handle the partially rigid classical degrees of freedom that occur in many systems of interest.

The new MD methods are based on the combination of reversible multiple time scale integration methods⁷ and the staging ansatz.^{2,8} The multiple time scale methods are used to treat the stiff harmonic forces present in the problem. The staging ansatz, originally developed for use in MC algorithms, is used here to narrow the frequency range present in the problem and thus decrease the time it takes to cover phase space. In the staging ansatz, one derives a noncanonical transformation from the Cartesian bead variables to a new set of "staging" variables. This transformation naturally divides the long and short wavelength modes present in the system and partially or completely diagonalizes the harmonic part of the action. Therefore, all the short wave-

length modes can be placed on the same time scale by simply adjusting the mass of their associated momenta. The advantage of the staging variables over the natural normal mode coordinates (which have been previously used in path integral MC calculations¹) is that the staging transformation has lower computational overhead. The related⁹ Fourier path integral Monte Carlo method^{1,10} can be similarly adapted to form an efficient MD scheme¹¹ but is not treated here.

The presence of stiff harmonic forces in path integral molecular dynamics (PIMD) requires that an ergodic canonical dynamics method be employed. Two different canonical schemes based on MD are considered, the Nosé-Hoover chain continuous-dynamics method and the stochastic hybrid Monte Carlo (HMC) method. The Nosé-Hoover chain method¹² is a new variant of the Nosé-Hoover extended system canonical dynamics algorithm.^{13,14} It has been shown to be ergodic for the type of stiff potential surface derived from the path integral action.¹² This is not the case for the simple Nosé-Hoover scheme.¹⁴ HMC¹⁵ grew out of early attempts to induce ergodic behavior^{6,16} in MD simulations by periodically resampling the particle velocities. This method also yields the canonical distribution (constant NVT).^{17,18} HMC uses the following procedure: (a) a new configuration is obtained from an old one by advancing the system with MD using a *reversible* integrator and a large time step; (b) the new configuration is accepted or rejected according to the usual Metropolis procedure; (c) if the new configuration is rejected, the momenta of the old configuration are resampled; (d) the process is repeated.¹⁵

In this paper, two new PIMD simulation methods, one based on the Nosé-Hoover chain method and the other on HMC, are developed utilizing the multiple time scale scheme and the noncanonical staging transformation described above. The methods are tested on a three dimensional quantum harmonic oscillator and an excess electron in fluid helium and xenon. The new approaches are found to give convergence rates comparable to those achieved by

^{a)}In partial fulfillment of the Ph.D. in the Department of Physics, Columbia University.

current PIMC algorithms and much greater than those achieved by the standard PIMD¹⁹ and/or standard PIHMC methods.¹⁵

II. METHODS

A. The staging method

The quantum mechanical partition function can be written as the trace of the density matrix²⁰⁻²³

$$\begin{aligned} Q(\beta) &= \int dx_1 \rho(x_1, x_1, \beta) \\ &= \int dx_1 \cdots dx_P \rho(x_1, x_2, \beta/P) \cdots \rho(x_P, x_1, \beta/P), \end{aligned} \quad (2.1)$$

where

$$\rho(x, x', \tau) = \langle x | e^{-\tau H} | x' \rangle, \quad (2.2)$$

$\beta = 1/kT$, and we have chosen to work in one dimension for simplicity. This expression is obtained using the idempotent property of the density matrix. The primitive high temperature density matrix approximation

$$\begin{aligned} \rho(x_i, x_{i+1}; \epsilon) &= \exp \left[-\frac{\epsilon V(x_i)}{2} \right] \rho_0(x_i, x_{i+1}; \epsilon) \\ &\quad \times \exp \left[-\frac{\epsilon V(x_{i+1})}{2} \right], \end{aligned} \quad (2.3)$$

where

$$\rho_0(x_i, x_{i+1}; \epsilon) = \left(\frac{m}{2\pi\hbar^2\epsilon} \right)^{1/2} \exp \left[-\frac{m}{2\hbar^2\epsilon} (x_i - x_{i+1})^2 \right] \quad (2.4)$$

can be substituted into Eq. (2.1) to yield

$$\begin{aligned} Q_P(\beta) &= \left(\frac{mP}{2\pi\hbar^2} \right)^{P/2} \int dx_1 \cdots dx_P \\ &\quad \times \exp \left(-\beta \sum_{i=1}^P \left[\frac{mP}{2\hbar^2\beta^2} (x_i - x_{i+1})^2 + \frac{1}{P} V(x_i) \right] \right). \end{aligned} \quad (2.5)$$

Here, m is the mass of the quantum particle, $V(x)$ is the potential energy, $x_{P+1} = x_1$ and $\epsilon = \beta/P$. Also, a distinction is made between the approximate partition function $Q_P(\beta)$ and the exact partition function $Q(\beta)$. The two agree formally in the limit that P goes to infinity, however, for large but finite P , agreement is found to be very good.^{1,4,21-23} Therefore, the index P will be suppressed in the future to avoid confusion.

In order to derive a MD and/or HMC algorithm, the configurational integral in Eq. (2.5) is written in the form of a phase space integral by introducing P momenta with mass, m_c ,^{3,6} conjugate to the coordinates. This mass is arbitrary and need not be equal to the true mass because thermodynamic averages do not depend on this quantity. Introducing the momenta, the partition function becomes

$$\begin{aligned} Q(\beta) &= f(m, m_c, \beta, P) \int dx_1 \cdots dx_P \int dp_1 \cdots dp_P \\ &\quad \times \exp \left(-\beta \sum_{i=1}^P \left[\frac{p_i^2}{2m_c} + \frac{mP}{2\hbar^2\beta^2} (x_i - x_{i+1})^2 \right. \right. \\ &\quad \left. \left. + \frac{1}{P} V(x_i) \right] \right), \end{aligned} \quad (2.6)$$

where the function $f(m, m_c, \beta, P)$ represents the overall normalization. The partition function in Eq. (2.6) looks like the classical partition function for a system of P interacting particles with Hamiltonian

$$H = \sum_{i=1}^P \left[\frac{p_i^2}{2m_c} + \frac{1}{2} m\omega_P^2 (x_i - x_{i+1})^2 + \frac{1}{P} V(x_i) \right], \quad (2.7)$$

where

$$\omega_P \equiv \frac{\sqrt{P}}{\beta\hbar}. \quad (2.8)$$

This is the Hamiltonian used in the primitive PIMD/PIHMC algorithm and is isomorphic to the Hamiltonian of a classical polymer chain with harmonic bonds between nearest neighbor beads in an external field, $V(x)$.⁴

The partition function need not be written or simulated in Cartesian coordinates. In fact, the nearest neighbor harmonic couplings that appear in Eq. (2.7) suggest that it may be inefficient to do so. In order to define a better coordinate system, the following identity taken from PIMC:^{2,8,24}

$$\begin{aligned} &\rho_0(x_1, x_2; \epsilon) \cdots \rho_0(x_j, x_{j+1}; \epsilon) \\ &= \prod_{k=2}^j \left(\frac{\beta m_k \omega_P^2}{2\pi} \right)^{1/2} \exp \left[-\frac{\beta}{2} m_k \omega_P^2 (x_k - x_k^*)^2 \right] \\ &\quad \times \left(\frac{m}{2\pi\hbar^2 j \epsilon} \right)^{1/2} \exp \left[-\frac{m}{2j\epsilon\hbar^2} (x_1 - x_{j+1})^2 \right], \end{aligned} \quad (2.9)$$

where

$$x_k^* = \frac{(k-1)x_{k+1} + x_1}{k} \quad (2.10)$$

and

$$m_k = m \left(\frac{k}{k-1} \right) \quad (2.11)$$

is used. This identity is proved by first using Eq. (2.4) to show that

$$\begin{aligned} &\left[\frac{\rho_0[x_1, x_k; (k-1)\epsilon] \rho_0(x_k, x_{k+1}; \epsilon)}{\rho_0(x_1, x_{k+1}; k\epsilon)} \right] \\ &= \left(\frac{\beta m_k \omega_P^2}{2\pi} \right)^{1/2} e^{-\beta/2 m_k \omega_P^2 (x_k - x_k^*)^2} \end{aligned} \quad (2.12)$$

and then converting the product of Eq. (2.9) to a product of terms similar to Eq. (2.12). The partition function can be rewritten in terms of N "segments" of chain length j using N such identities. The $N(j-1)$ intermediate beads (beads $2 \cdots j, j+2 \cdots 2j, \cdots$) are referred to as the staging beads; the others (beads $1, j+1, 2j+1, \cdots$) as "end point" beads. The staging beads have masses defined by Eq. (2.11) which are called the *staging masses*, while the end point beads have masses equal to the actual particle mass,

m . Let the set of staging and endpoint masses be denoted $\{m_i\}$. The parameters N and j must be chosen such that $Nj = P$.

$$(2.13)$$

Substitution of the N identities into the partition function yields

$$Q(\beta) = \left(\frac{\beta m \omega_j^2}{2\pi} \right)^{N/2} \prod_{k=2}^j \left(\frac{\beta m_k \omega_P^2}{2\pi} \right)^{N/2} \int dx_1 \cdots dx_P \\ \times \exp \left[- \sum_{s=0}^{N-1} \frac{\beta}{2} m \omega_j^2 (x_{s \cdot j+1} - x_{(s+1) \cdot j+1})^2 \right. \\ \left. - \sum_{s=0}^N \sum_{k=2}^j \frac{\beta}{2} m_k \omega_P^2 (x_{s \cdot j+k} - x_{s \cdot j+k}^*)^2 \right] \\ \times \exp \left[- \frac{\beta}{P} \sum_{i=1}^P V(x_i) \right], \quad (2.14)$$

where

$$\omega_j \equiv \frac{1}{\beta \hbar} \sqrt{\frac{P}{j}} \quad (2.15)$$

and

$$x_{s \cdot j+k}^* = \frac{(k-1)x_{s \cdot j+k+1} + x_{s \cdot j+1}}{k}. \quad (2.16)$$

A linear transformation is defined,

$$u_{s \cdot j+1} = x_{s \cdot j+1}, \\ u_{s \cdot j+k} = x_{s \cdot j+k} - x_{s \cdot j+k}^* \quad (2.17)$$

with inverse

$$x_{s \cdot j+1} = u_{s \cdot j+1} \\ x_{s \cdot j+k} = \sum_{l=k}^{j+1} \frac{k-1}{l-1} u_{s \cdot j+l} + \frac{j-k+1}{j} u_{s \cdot j+1}. \quad (2.18)$$

The inverse can also be expressed as a recursion

$$x_{s \cdot j+k} = u_{s \cdot j+k} + \frac{k-1}{k} x_{s \cdot j+k+1} + \frac{1}{k} x_{s \cdot j+1}. \quad (2.19)$$

A change of variables from x to u plus the introduction of momenta conjugate to the u 's yields

$$Q(\beta) = f(m, m', \beta, P) \int du_1 \cdots du_P \int dp_1 \cdots dp_P \\ \times \exp \left[- \beta \sum_{i=1}^P \frac{p_i^2}{2m_i'} - \sum_{s=0}^{N-1} \frac{\beta}{2} m \omega_j^2 (u_{s \cdot j+1} \right. \\ \left. - u_{(s+1) \cdot j+1})^2 \right] \exp \left[- \sum_{s=0}^N \sum_{k=2}^j \frac{\beta}{2} m_k \omega_P^2 u_{s \cdot j+k}^2 \right. \\ \left. - \frac{\beta}{P} \sum_{i=1}^P V[x_i(u)] \right], \quad (2.20)$$

where the function $f(m, m', \beta, P)$ contains the normalization constant. The Jacobian for the transformation is unity. The following Hamiltonian which we call the staging Hamiltonian can be derived from the partition function, Eq. (2.20):

$$H = \sum_{i=1}^P \frac{p_i^2}{2m_i'} + \sum_{s=0}^{N-1} \frac{1}{2} m \omega_j^2 (u_{s \cdot j+1} - u_{(s+1) \cdot j+1})^2 \\ + \sum_{s=0}^N \sum_{k=2}^j \frac{1}{2} m_k \omega_P^2 u_{s \cdot j+k}^2 + \frac{1}{P} \sum_{i=1}^P V[x_i(u)]. \quad (2.21)$$

The possibility that the fictitious masses $\{m_i'\}$ are different from the actual bead masses $\{m_i\}$ has been taken into account. In the limit $j=P$, $N=1$, the nearest neighbor coupling is completely diagonalized, so that the chain reduces to a collection of independent harmonic oscillators coupled only through the external potential. Note that the derivative of the potential energy with respect to the staging variables can be expressed in terms of the primitive forces ($F_i = -\partial V/\partial x_i$) as

$$\frac{\partial V}{\partial u_{s \cdot j+1}} = \frac{\partial V}{\partial x_{s \cdot j+1}} + \sum_{l=2}^j \frac{j-l+1}{j} \frac{\partial V}{\partial x_{s \cdot j+l}} \\ + \sum_{l=2}^j \frac{l-1}{j} \frac{\partial V}{\partial x_{(s-1) \cdot j+l}}, \\ \frac{\partial V}{\partial u_{s \cdot j+k}} = \sum_{l=2}^k \frac{l-1}{k-1} \frac{\partial V}{\partial x_{s \cdot j+l}} \quad (2.22)$$

or recursively as

$$\frac{\partial V}{\partial u_{s \cdot j+1}} = \frac{\partial V}{\partial x_{s \cdot j+1}} + \sum_{l=2}^j \frac{\partial V}{\partial x_{(s-1) \cdot j+l}} \\ - \frac{j-1}{j} \left[\frac{\partial V}{\partial u_{(s+1) \cdot j}} - \frac{\partial V}{\partial u_{(s-1) \cdot j}} \right], \\ \frac{\partial V}{\partial u_{s \cdot j+k}} = \frac{\partial V}{\partial x_{s \cdot j+k}} + \frac{k-2}{k-1} \frac{\partial V}{\partial u_{s \cdot j+k-1}}, \quad (2.23)$$

where $x_{-j+1} = x_{(N-1) \cdot j+1}$, $x_{N \cdot j+1} = x_1$ and $x_0 = x_P$.

The staging Hamiltonian Eq. (2.21) is different from the primitive Hamiltonian, Eq. (2.7). The fact that only configurational averages are desired has been used to construct a new Hamiltonian with no canonical transformation relating it to the primitive Hamiltonian. The two Hamiltonians will thus yield different trajectories when used in MD or HMC calculations and hence give different convergence rates for various averages.

The staging coordinates have advantages over both the usual Cartesian coordinates and the natural normal mode coordinates which are also sometimes used in path integral calculations.¹ Within the staging ansatz it is easy to adjust the masses of the beads (the $\{m_i'\}$), such that all the staging beads or modes in the chain have the same frequency. This will clearly increase the convergence of time averages as all these modes will be sampled at the same rate. In general, it is not desirable to have all modes move on the same time scale. In a rapidly varying external potential, fast fluctuations of the long wavelength modes will require a small MD time step for stable integration. The staging method handles this problem by introduction of the variable j , which naturally classifies the modes and allows only those with wavelength smaller than some cutoff to fluctuate rapidly. Such a division of time scales based on wavelength can also be constructed using the normal modes.

The principal advantage of the staging coordinates over the natural normal modes is that the staging transformations, $u \rightarrow x$ and $x \rightarrow u$ as well as the transformation of the forces have simple recursive forms. This is not the case for the natural normal modes of a cyclic polymer chain.

B. Method of integration

The use of the MD or HMC method to calculate path integrals has proved to be troublesome for two reasons. First, for systems in which quantum mechanical effects are important, a large value of P will be needed to converge the partition function. As Eqs. (2.7) and (2.21) suggest, the harmonic contribution to the total force increases linearly with P , while the external force decreases as $1/P$. The increase in force constant relative to the external force with P means that a smaller time step must be used, and thus, more time is required for the stable integration of the harmonic motion as the system becomes more quantum mechanical. That is, the time step must be reduced only to integrate the uninteresting harmonic part of the action. In addition, in PIMD simulations equipartitioning will be slow and it will be extremely difficult to insure that canonical ensemble averages are obtained.⁶

Nosé-Hoover dynamics can, in principle, generate trajectories whose time average will give the canonical ensemble average.^{13,14,25} However, the method fails for systems such as the one dimensional harmonic oscillator.¹⁴ This is an important point, as the one dimensional quantum mechanical free particle can be written as $P-1$ uncoupled oscillators and one classical free particle. However, it has recently been shown that a variant of the method can be used alleviate this difficulty.¹² In this new method, the Nosé-Hoover chain method, the usual Nosé-Hoover equations of motion are supplemented by a set of thermostats which successively thermostat each other

$$\begin{aligned} \dot{q} &= \frac{P}{m}, \\ \dot{p} &= -\frac{\partial V(q)}{\partial q} - P \frac{p_{\eta_1}}{Q_1}, \\ \dot{\eta}_i &= \frac{p_{\eta_i}}{Q}, \\ \dot{p}_{\eta_1} &= \left[\frac{p^2}{m} - kT \right] - p_{\eta_1} \frac{p_{\eta_2}}{Q}, \\ \dot{p}_{\eta_j} &= \left[\frac{p_{\eta_{j-1}}^2}{Q} - kT \right] - p_{\eta_j} \frac{p_{\eta_{j+1}}}{Q}, \\ \dot{p}_{\eta_M} &= \left[\frac{p_{\eta_{M-1}}^2}{Q} - kT \right]. \end{aligned} \quad (2.24)$$

Here M is the number thermostats included and the optimal choice for thermostat mass is $Q = kT/\omega^2$ where ω is some representative frequency of the potential $V(q)$. The dynamics, Eqs. (2.24), has the conserved energylike quantity

$$H' = \frac{p^2}{2m} + V(q) + \sum_{i=1}^M \left[\frac{p_i^2}{2Q} + kT\eta_i \right], \quad (2.25)$$

where H' is not a proper Hamiltonian for the system. For values as small as $M=2$, the canonical ensemble is obtained for a one dimensional harmonic oscillator. Therefore, to insure that canonical averages will be generated in the path integral simulations, each bead in the path integral polymer will be given its own independent Nosé-Hoover chain. Indeed, for the three dimensional systems studied in this paper, each degree of freedom of the beads will be given a Nosé-Hoover chain, for a total $3P$ chains. While this may seem like a very large number of degrees of freedom, the time required to evaluate the Nosé forces is a negligible fraction of the total simulation time. The primitive or staging PIMD algorithms are then generated by substituting the primitive/staging forces into the multidimensional analog of Eqs. (2.24). The conserved quantity is then that which corresponds to Eq. (2.25). In HMC simulations, Nosé-Hoover chains are not used, but rather just the straightforward Newtonian dynamics derived from Eq. (2.7) or Eq. (2.21).

The reversible reference system propagator algorithm (RESPA)⁷ can be used to eliminate the time scale problems associated with the harmonic bonds. This method is based on a Trotter expansion of the classical propagator, $\exp(iLt)$. Consider the Liouville operator (in the absence of any Nosé thermostats)

$$iL = \dot{x} \frac{\partial}{\partial x} + [F_h(x) + \Delta F(x)] \frac{\partial}{\partial p}, \quad (2.26)$$

where $F_h(x)$ represents the harmonic force and $\Delta F(x)$ the force due to the true external potential $V(x)$. The system is evolved for time step Δt by applying the classical propagator, $\exp(iL\Delta t)$, to an initial state. A multiple time scale algorithm is obtained by applying the Trotter expansion of the evolution operator

$$\begin{aligned} \exp(iL\Delta t) &= \exp \left[\Delta F(x) \frac{\partial}{\partial p} \frac{\Delta t}{2} \right] \exp(iL_h \Delta t) \\ &\quad \times \exp \left[\Delta F(x) \frac{\partial}{\partial p} \frac{\Delta t}{2} \right] + \mathcal{O}(\Delta t^3), \end{aligned} \quad (2.27)$$

to the state $\{x(0), \dot{x}(0)\}$. The following equations of motion are obtained:

$$\begin{aligned} x(\Delta t) &= x_h \left[\Delta t; x(0), \dot{x}(0) + \frac{\Delta t}{2m} \Delta F[x(0)] \right], \\ \dot{x}(\Delta t) &= \dot{x}_h \left[\Delta t; x(0), \dot{x}(0) + \frac{\Delta t}{2m} \Delta F[x(0)] \right] \\ &\quad + \frac{\Delta t}{2m} \Delta F[x(\Delta t)], \end{aligned} \quad (2.28)$$

where $\{x_h, \dot{x}_h\}$ refers to the position and velocity generated under the action of $\exp(iL_h \Delta t)$. The action of $\exp(iL_h \Delta t)$ on the initial state is determined numerically to order $\Delta t^3/n^2$ by writing this operator as $[\exp(iL_h \Delta t/n)]^n$ and applying the velocity Verlet algorithm with time step $\delta t = \Delta t/n$, n times.^{7,26} Therefore, as the harmonic frequency increases, the parameter n can be increased with Δt held constant to yield the same level of energy conservation. There is some overhead associated with an increased number of harmonic force evaluations as n is increased, but this is more than

offset by the cost of evaluating the external force. In this manner, the stiff harmonic forces in path integrals can be handled efficiently. The algorithm can be directly applied to the HMC method which uses the Newtonian equations of motion. In Appendix A, the algorithm is modified for use with systems undergoing Nosé–Hoover chain dynamics.

C. Definition of parameters

In order to fully define the staging PIMD and/or PIHMC algorithms as described above, several parameters must be specified. These parameters include the masses of the Nosé–Hoover thermostats (MD is defined to refer to Nosé–Hoover chains dynamics), the value of j , the RESPA parameters Δt and n , and the masses of the path integral beads themselves, the $\{m'_i\}$. The staging thermostat mass, the mass of the thermostat on the staging beads, is taken to be $Q_{\text{stage}} = kT/\omega_P^2$, while the mass of the thermostat on the end point beads, is taken to be the smallest value that does not degrade energy conservation for given j . A good first guess is $j \cdot Q_{\text{stage}}$. The parameter j is chosen to be the largest value that does not degrade energy conservation in staging PIMD. In staging PIHMC, j is chosen to give the most rapid convergence. Though this procedure sounds time consuming, it is actually fairly straightforward to implement. In staging PIMD, as j is increased from an initial value there is a well defined cutoff where energy conservation will begin to break down. Once this value is obtained, Q_{end} can be reduced from $j \cdot Q_{\text{stage}}$. The adjustment of the RESPA parameters Δt and n is also fairly straightforward. For j less than its cutoff, Δt determines the energy conservation for n greater than another cutoff value. Thus n is set to the smallest value possible that maintains energy conservation. In HMC, n is chosen so that the acceptance probability is solely determined by Δt . Again, there is a well defined cutoff value. The last parameter that must be fixed is the choice of the path integral mass. If there is no motion other than that of the path integral itself, $\{m'_i\} = \{m_i\}$ is a good choice. In the presence of other motion, classical solvent degrees of freedom for example, the masses should be taken to be $\{m'_i\} = \{Cm_i\}$ where C is the largest possible value that does not degrade energy conservation or in HMC the acceptance probability. In practice, it should make Δt equal to the time step for the solvent. Again, despite the seemingly large number of parameters, it only takes a few short runs to determine them. In addition, once the parameters are chosen, if the number of beads is increased, everything scales accordingly so that the adjustment procedure is only performed once.

D. Staging path integral Monte Carlo

The staging PIMC method incorporates the staging ansatz described above into MC. Here $(j-1)$ beads are directly sampled between fixed end points according to the free particle action using the staging transformations defined above [cf. Eq. (2.17)]. The move is accepted or rejected according to the usual Metropolis procedure.^{2,27}

This effectively eliminates the harmonic bonds from the problem (i.e., they have been directly sampled.) Note, the first end point bead is chosen at random and the second determined by j and the periodicity of the polymer chain. The parameter j is chosen so that the acceptance probability is 40%. A staging PIMC pass is defined as $P/(j-1)$ moves of $(j-1)$ beads.

E. Path integral hybrid Monte Carlo

Hybrid Monte Carlo (HMC) is a combined MD-MC method that can be used to obtain the canonical distribution.¹⁵ The method generates a new configuration from an old configuration by integrating the Newtonian equations of motion with a *reversible* numerical integrator and a large time step. The move is then accepted or rejected according to the usual Metropolis procedure²⁸ based on $e^{-\beta\Delta H}$, where ΔH is the change in the total energy as a result of the move. The integrator must be reversible in order to satisfy the microscopic reversibility requirement of the Metropolis MC method.²⁸ If a move is rejected, then new momenta are then directly sampled from the Boltzman distribution. The procedure is repeated many times to cover phase space.

The HMC method can be used with any Hamiltonian and can thus be applied to either the staging or the primitive path integral ansatz [i.e., Eq. (2.20) or Eq. (2.7)]. HMC simply replaces Nosé–Hoover dynamics as the method used to generate the canonical distribution. In both the primitive and staging PIHMC, the reversible multiple time step integrator, RESPA may be used. A small time step is chosen to integrate the harmonic piece of the action accurately and the large step is chosen such that 40% of the moves are accepted. Larger acceptance probabilities are found to be less efficient. However, when RESPA is not used, higher acceptance probabilities ($\sim 90\%$) are found to give most rapid coverage of phase space.

In staging PIHMC, a modification of the standard method is necessary, to achieve maximum efficiency. At each step an integer random number between zero and $(j-1)$ is chosen and the Cartesian coordinate labels (the x 's) are reassigned by rotating the coordinate labels around the cyclic polymer chain by this amount ($x_i \rightarrow x_{i+r}$ where $x_{i+p} = x_i$). This move does not change the action and is accepted with probability one. New staging coordinates (the u 's) are then calculated using the rotated Cartesian coordinate labels [cf. Eq. (2.17)]. This reassigning of the coordinate labels has the effect of periodically changing the frequency scale of a given bead. If a bead was initially an end point, after reassignment it is likely to become a staging bead, thus insuring that no single bead remains a fast or slow bead permanently. This helps each bead to sample its available phase space more efficiently. The reassignment scheme was also tested in staging PIMD simulations under Nosé–Hoover dynamics but was found to have no effect on the convergence of statistical averages.

III. MODEL PROBLEMS

Several model problems were considered to thoroughly test the new methods, the 3D quantum mechanical harmonic oscillator, an excess electron in fluid helium and an

excess electron in fluid xenon. The oscillator is studied because it is a simple, computationally inexpensive model uncomplicated by a large number of parameters. It nonetheless has all the problems associated with path integral simulations, stiff harmonic bonds, nonergodic behavior, etc. It is used to demonstrate the new methods and in particular to show the importance of using multiple time scale integration and the staging variable transformation. Electrons in fluid helium and xenon are realistic systems that involve the motion of additional classical degrees of freedom (solvent). Both helium and xenon are studied in order to compare the methods in contrasting environments; in helium, the electron is localized in a cavity devoid of solvent while in xenon it extended throughout the fluid. Solvent motion plays an important part in both systems. Therefore, the efficiency of the path integral methods are compared for both frozen equilibrated solvent configurations as well as for the full problem. In addition, the ability of HMC, MD, and MC to sample the pure solvent degrees of freedom is examined.

The parameters of the oscillator were taken to be $\beta\hbar\omega = 15.8$, $m\omega/\hbar = 0.03$, $P = 400$ which defines a quantum mechanical ground state dominated system.²⁹ The excess electron in liquid helium, another quantum mechanical ground state dominated system, was studied using a system of $N = 256$ helium atoms and a single excess electron in a periodic cubic box. The same number of atoms was used to study an electron in liquid xenon. The solvent atoms interact through Lennard-Jones potentials with $\epsilon_{\text{He}} = 10.22$ K, $\sigma_{\text{He}} = 2.556$ Å, $\epsilon_{\text{Xe}} = 229.15$ K and $\sigma_{\text{Xe}} = 4.332$ Å, respectively. The temperature and the density of the both systems was taken to be $T = 309$ K and $\rho\sigma^3 = 0.5$.²⁷ The electron interacts with the helium and xenon atoms via a pseudo-potential²⁷

$$V(r) = \frac{A}{r^4} \left[\frac{B}{C + r^6} - 1 \right], \quad (3.1)$$

with $A_{\text{He}} = 0.665$, $B_{\text{He}} = 89\,099.0$, $C_{\text{He}} = 12\,608.0$, $A_{\text{Xe}} = 12.59$, $B_{\text{Xe}} = 4920$, and $C_{\text{Xe}} = 3793$ all in atomic units.²⁷ The electron was discretized with $P = 990$ beads and energy conservation in PIMD is monitored by the formula⁷

$$\Delta E = \frac{1}{N_T} \sum_{i=1}^{N_T} \left| \frac{E_i - E_0}{E_0} \right|, \quad (3.2)$$

where N_T is the total number of time steps.

The staging PIMD simulations of the harmonic oscillator were integrated with a big time step of $\Delta t = 0.19\omega_P$ and a small time step $\delta t = \Delta t/5$, respectively. The other parameters are taken to be $j = 100$ and $Q_{\text{stage}} = kT/\omega_P^2$, $Q_{\text{end}} = 50Q_{\text{stage}}$, $M = 2$. For PIMD simulations based on the primitive algorithm, we set $\Delta t = 0.38\omega_P$, $\delta t = \Delta t/10$ and $Q = kT/\omega_P^2$, $M = 2$. In both staging PIMD and primitive PIMD simulations, the energy conservation, as measured by Eq. (3.2) was set to 1×10^{-4} . The staging PIMC simulations used $j = 80$. The PIHMC studies of three dimensional oscillator employed time steps of $\Delta t = 0.91\omega_P$, $\Delta t = 19.0\omega_P$ for staging PIHMC (with $j = 100$) and the primitive PIHMC, respectively. The inner or small time step was fixed at $\delta t = 0.038\omega_P$ as in the staging PIMD sim-

ulations. Simulations using primitive PIHMC without multiple time step integration utilized a time step of $\Delta t = 0.36\omega_P$.

The staging PIMD simulations of the excess electron in fluid helium and xenon were integrated using $\Delta t = 1.25$ a.u., $\delta t = \Delta t/3$, $j = 66$, $M = 2$, $Q_{\text{end}} = 67.32$, $Q_{\text{stage}} = 1.02$. A single Nosé-Hoover chain consisting of 4 thermostats was used to control the temperature of the solvent. The masses of these thermostats were set equal to $Q_1 = 3NkT/\omega_{\text{LJ}}^2$ and $Q_i = kT/\omega_{\text{LJ}}^2$ ($i = 2, 3, 4$) where ω_{LJ} is the frequency in the Lennard-Jones well, $m_{\text{He}}\omega_{\text{LJ}}^2 = 8 \times 10^{-5}$ for helium and $m_{\text{Xe}}\omega_{\text{LJ}}^2 = 7 \times 10^{-4}$ for xenon in atomic units. The mass of the helium atom was set to 0.156 a.u. and the mass of the xenon atom was set equal to 0.33 a.u. These masses are the smallest possible that can be used without significantly degrading the energy conservation for the choice of j described above. The energy conservation of the simulations as measured by Eq. (3.2) are then $\Delta E = 1 \times 10^{-3}$ for helium and $\Delta E = 1 \times 10^{-4}$ for xenon. The tolerance for used in the high temperature helium is a bit high but it is difficult to achieve better results at such a high temperature and maintain a reasonable time step.

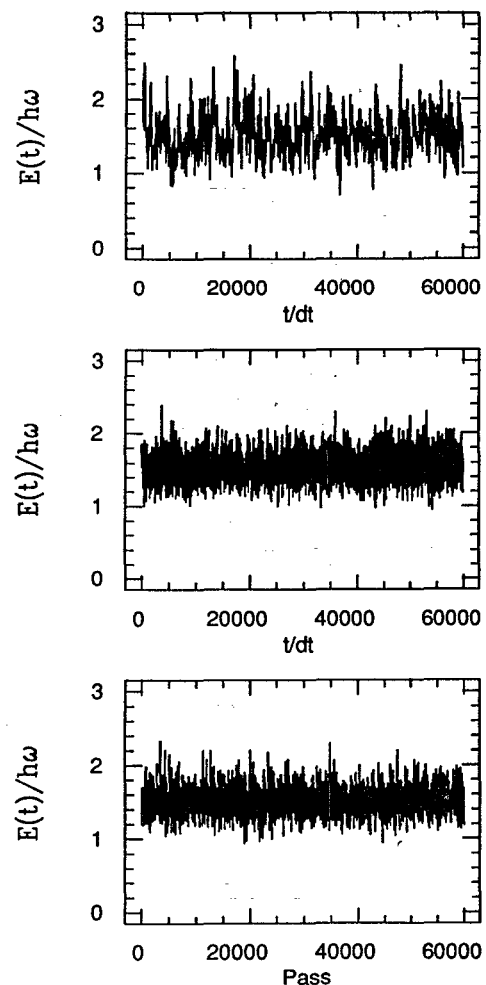


FIG. 1. The instantaneous fluctuations in the Virial estimator averaged over 20 steps obtained from simulations of the three dimensional harmonic oscillator using primitive PIMD (upper), staging PIMD (middle) staging PIMC (lower).

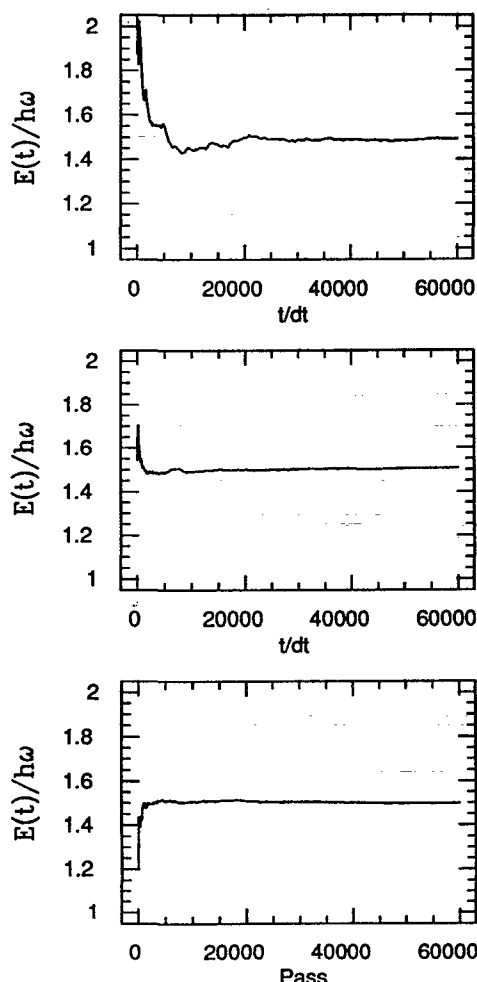


FIG. 2. The cumulative average of the Virial estimator obtained from simulations of the three dimensional harmonic oscillator using primitive PIMD (upper), staging PIMD (middle), staging PIMC (lower).

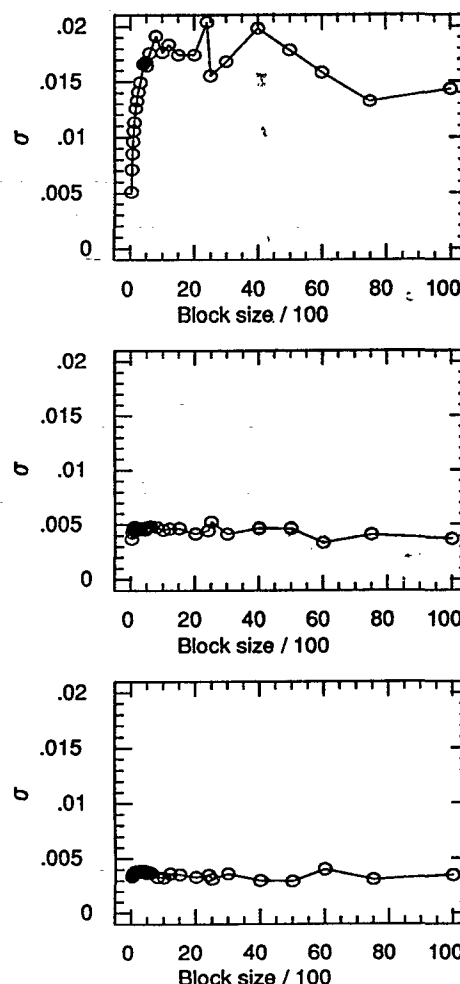


FIG. 3. The error as a function of block size in the Virial estimator obtained from simulations of the three dimensional harmonic oscillator using primitive PIMD (upper), staging PIMD (middle) staging PIMC (lower).

The masses and values of the j parameters selected for PIMD are also used in the staging PIHMC simulations of electrons in helium and xenon. However, the time steps were taken to be $\Delta t = 7.25$ a.u., $\delta t = \Delta t/17$ for helium and $\Delta t = 6.0$ a.u., $\delta t = \Delta t/14$ for xenon.

The staging PIMC simulations of excess electron in helium used moves of length $j=55$ beads to sample the electronic coordinate and a step of size of 4.5 a.u. to move the helium atoms. For xenon, the corresponding parameters are $j=59$ and a step size of 3.44 a.u.

In order to study convergence of the methods, the instantaneous fluctuations of the virial estimator^{23,30} was monitored. For a bound system such as a harmonic oscillator, the virial estimator is given by

$$E_P = \frac{1}{P} \sum_{i=1}^P \left[V(\mathbf{r}_i) + \frac{1}{2} \mathbf{r}_i \cdot \nabla_i V(\mathbf{r}_i) \right] \quad (3.3)$$

while for open systems the formula becomes

$$E_P = \frac{1}{P} \sum_{i=1}^P \left[V(\mathbf{r}_i) + \frac{3}{2\beta} + \frac{1}{2} (\mathbf{r}_i - \mathbf{r}_c) \cdot \nabla_i V(\mathbf{r}_i) \right], \quad (3.4)$$

where $\mathbf{r}_c = 1/P \sum_{i=1}^P \mathbf{r}_i$ is the path integral centroid. For all the examples, an initial configuration was equilibrated for 2500 steps, and averages were computed for 10 000 steps.

IV. RESULTS

A. Harmonic oscillator

Simulations were carried out on the three dimensional quantum mechanical harmonic oscillator using staging PIMD, primitive PIMD (including RESPA and the Nosé-Hoover chains) and staging PIMC. In Fig. 1, the instantaneous fluctuations in the virial estimator (averaged over 20 steps) obtained from the simulations are plotted. The primitive PIMD method shows fluctuations that are generally larger and slower than those obtained using either the staging PIMD or the staging PIMC method. On the other hand, the staging PIMD and the staging PIMC methods exhibit comparable fluctuations in the estimator. In Fig. 2, the convergence of the cumulative average of the virial estimator is shown for the three methods. Again, it appears that the primitive PIMD method converges more

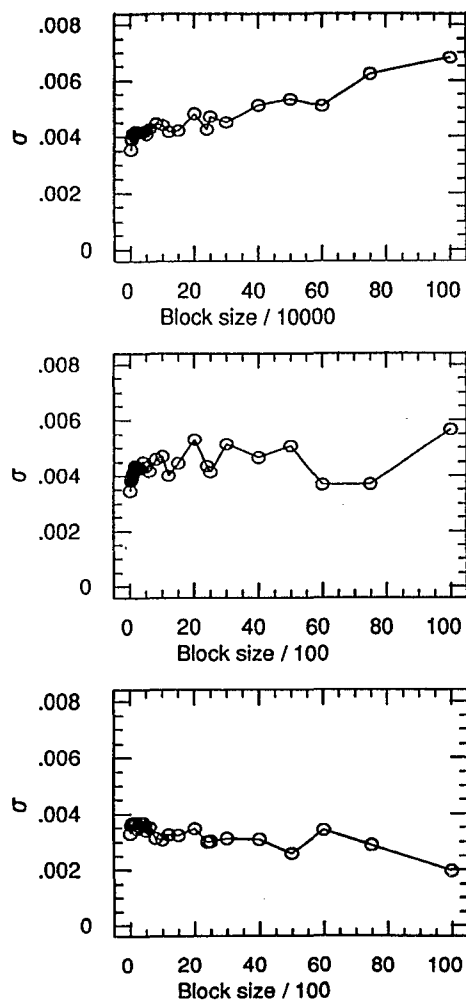


FIG. 4. The error as a function of block size in the Virial estimator obtained from simulations of the three dimensional harmonic oscillator using primitive PIHMC (upper), primitive PIHMC with multiple time step integration (middle), staging PIHMC ($j=100$) with multiple time step integration (lower).

slowly than either the staging PIMD or the staging PIMC method. In Fig. 3, the relative error in the mean [see Eq. (2.2) of Ref. 30] for the virial estimator as a function of block size is plotted for the three methods.³¹ This quantity gives a detailed measure of the efficiency of the algorithms (i.e., how many more configurations would have to be sampled in order to achieve the same degree of accuracy). Staging PIMD is about 1.6 times less efficient than staging PIMC while primitive PIMD is about a factor of 20 times less efficient than staging PIMC. Without RESPA, primitive PIMD would be a factor of 200 times less efficient than staging PIMC. It should be noted that replacing the Nosé-Hoover chain scheme with a stochastic heat bath algorithm^{6,18} (the method of choice for typical primitive PIMD simulations) results in a much less efficient algorithm.

The HMC method¹⁵ was also studied. In Fig. 4, the error bar as a function of block size is presented for primitive PIHMC without multiple time step integration, primitive PIHMC with multiple time step integration and staging PIHMC ($j=100$). Primitive PIHMC without multiple

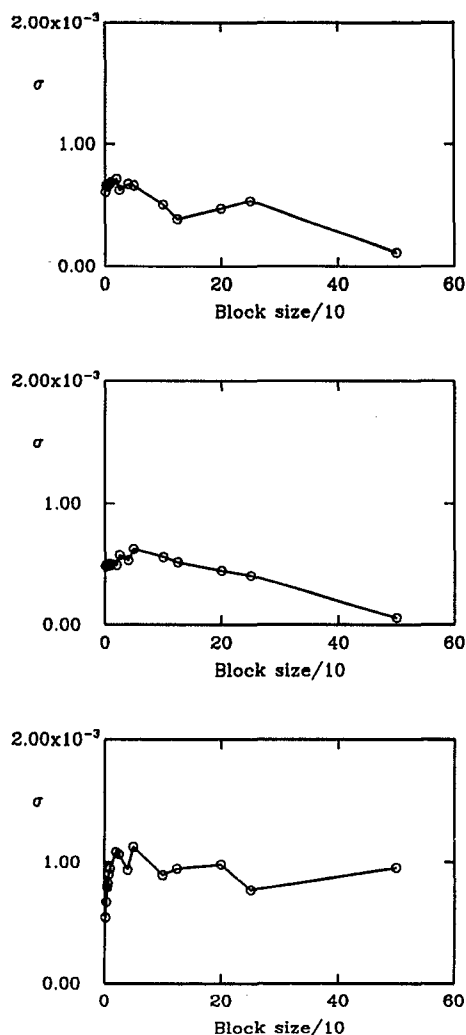


FIG. 5. The error as a function of block size in the Virial estimator obtained from simulations of an excess electron in a frozen equilibrated helium configuration using staging PIMD (upper), staging PIMC (middle) staging HMC (lower).

time step integration is 150 times less efficient than staging PIMC. When multiple time integration is included the method becomes almost as efficient as PIMC. Staging increases the efficiency of the PIHMC method to equal that of PIMC. It also reduces the overhead due to the integration of the reference system by a factor of 20. Interestingly, without the rotation move outlined in the methods section, staging PIHMC with multiple time step integration is slightly less efficient than the primitive method with multiple time step integration. Despite these results, the HMC method remains somewhat limited. The method cannot be used to study systems that have constraints, as the usual integrators (shake or shake/rattle) are not reversible.

B. Excess electron in liquid helium and xenon

Single excess electrons in fluid helium and xenon were also studied. In Fig. 5, the error bar for the virial estimator as a function of block size is shown for an excess electron in a frozen equilibrated helium configuration for the staging PIMD, staging PIMC and staging PIHMC methods.

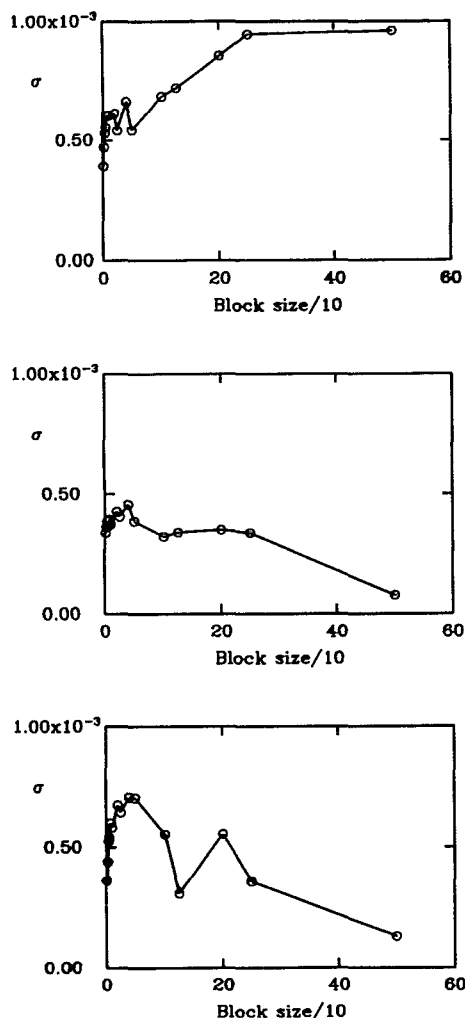


FIG. 6. The error as a function of block size in the Virial estimator obtained from simulations of an excess electron in a frozen equilibrated xenon configuration using staging PIMD (upper), staging PIMC (middle), staging PIHMC (lower).

An equilibrated configuration is obtained from a full staging PIMD simulation of the combined system (i.e., both electron and fluid moving). The error bars are comparable for the three methods, although from the ratio of the square of the error bars, PIMC is about a factor of 1.6 better than PIMD, similar to the oscillator case. In Fig. 6, the error bar as a function of block size for an excess electron in a frozen equilibrated xenon configuration is shown for the three methods. Again, the error bars are found to be roughly similar with PIMC about a factor of 1.6 better than PIMD from the ratio of the square of the error bars.

The ability of the three methods to treat the neat helium and xenon fluids at the conditions of interest is considered next. In Fig. 7, the mean square displacement vs time step/pass produced by each of the three methods, HMC, MD, and MC is shown for helium at $T^*=30.23$ and $\rho^*=0.5$ (see Sec. III). Here all references to molecular dynamics (MD) indicate Nosé-Hoover chain dynamics (see Sec. III). The results indicate that HMC is

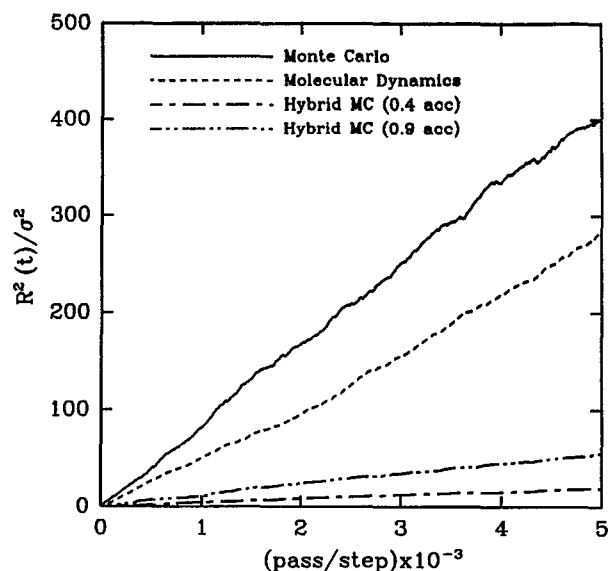


FIG. 7. The mean square displacement divided by the square of the Lennard-Jones σ for helium as a function of time step/pass for MC, MD, HMC at 90% acceptance, and HMC at 40% acceptance for pure helium ($T^*=30.23$ and $\rho^*=0.5$).

not competitive with either MD or standard MC. Therefore, HMC will not sample the available phase space as efficiently as either of the other two methods. Also, the mean square displacement of MD is less than that of MC by a small but significant amount; the ratio of the per time step/pass diffusion constants is a factor of 1.4. It can therefore be expected, that in a full simulation of an electron in fluid helium, the error bar for MC would be smaller than that of MD and much smaller than that of HMC. In Fig. 8, the mean square displacement vs time step/pass pro-

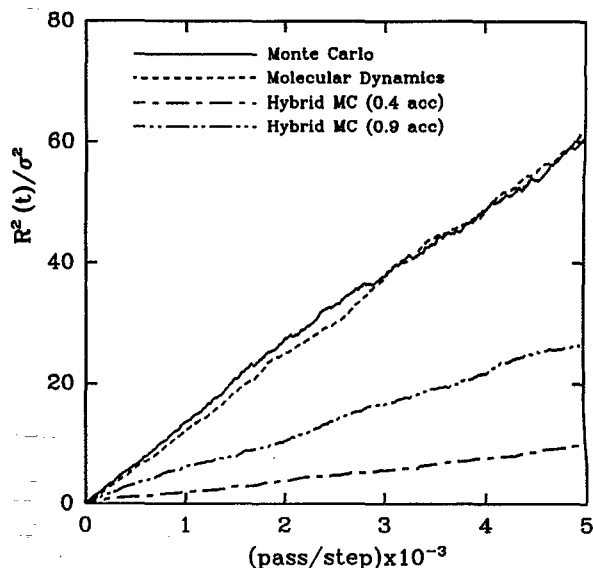


FIG. 8. The mean square displacement divided by the square of the Lennard-Jones σ for xenon as a function of time step/pass for MC, MD, HMC at 90% acceptance, and HMC at 40% acceptance for pure xenon ($T^*=1.4$ and $\rho^*=0.5$).

duced by each of the three methods, HMC, MD, and MC is shown for xenon at $T^*=1.4$ and $\rho^*=0.5$ (see Sec. III). In this case, MD and MC give essentially the same mean square displacement. Again, however, HMC does not give as large a mean square displacement as either MC or MD. In Appendix C, an explanation for the failure of HMC on the pure fluid is proposed. Given the poor performance of HMC in treating the pure solvent, it is not used in full simulations of the electron in helium and xenon discussed below.

The results of the full simulations of the electron in liquid helium and liquid xenon are shown in Figs. 9 and 10, respectively. As expected, the error bar for the staging PIMC calculation of the electron in liquid helium is smaller than that calculated with staging PIMD. The square of the ratio of the error bar for staging PIMC to that of staging PIMD is roughly a factor of 1.6 indicating that staging PIMC is 1.6 times more efficient than staging PIMD, again, comparable to the oscillator case. In xenon, the square of the ratio of error bars of staging PIMD to staging PIMC is roughly a factor of 1.5 which again indicates that staging PIMC is 1.5 times more efficient than staging PIMD for this particular system.

V. CONCLUSIONS

A new PIMD algorithm (the staging PIMD method) has been developed. The method which employs the Nosé–

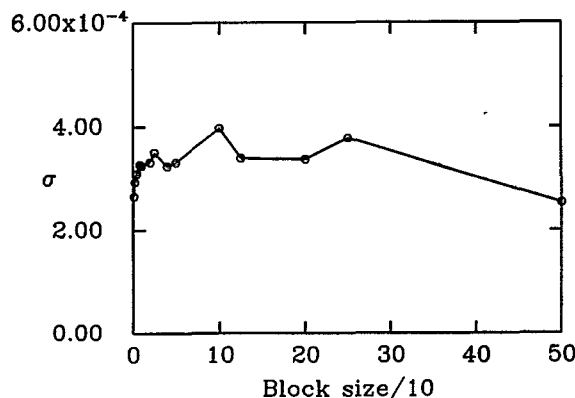
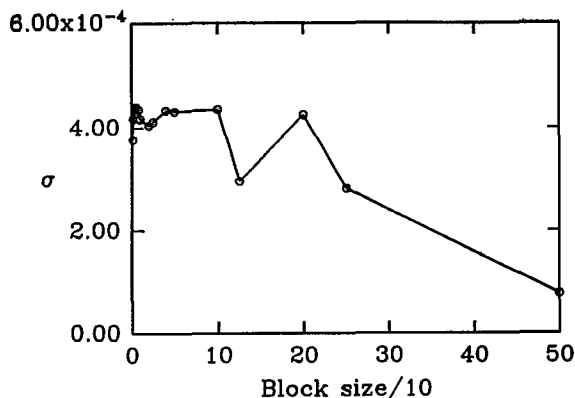


FIG. 9. The error as a function of block size in the Virial estimator obtained from full simulations of an excess electron in liquid helium using staging PIMD (upper) staging PIMC (lower).

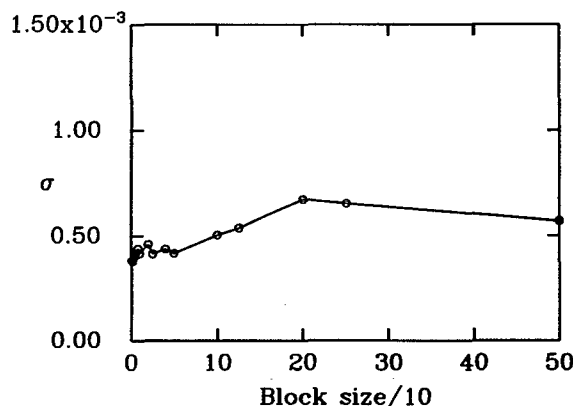
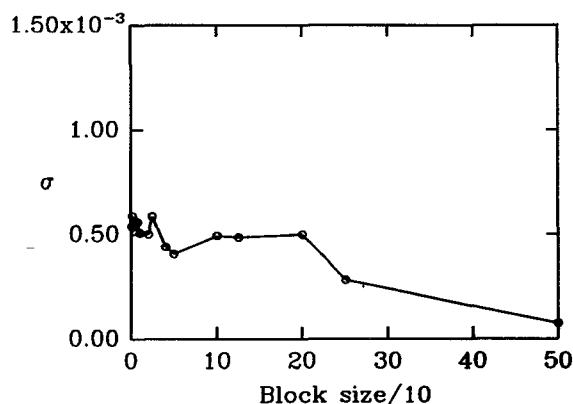


FIG. 10. The error as a function of block size in the Virial estimator obtained from full simulations of an excess electron in liquid xenon using staging PIMD (upper) staging PIMC (lower).

Hoover chain dynamics¹² and the multiple time scale integration scheme RESPA⁷ is about as efficient (less efficient by about a factor of 1.6) as the best PIMC method and much more efficient ($200\times$) than the basic PIMD method. The new method is straightforward to implement and can be incorporated into existing codes with little difficulty.

A new PIHMC method is also developed. When multiple time scale integration techniques are used, the method is as efficient as PIMC and the new staging PIMD algorithm. This method also requires the rotation of the coordinate labels as discussed in Sec. II E. This rotation of coordinate labels was also tested in the staging PIMD method with Nosé–Hoover chains and was found to make no significant improvement in its efficiency. HMC appears to perform poorly on the pure Lennard-Jones fluids. Therefore, the method is not recommended for use in systems which include solvent motion without additional methodological developments. Also, the HMC method cannot be used to study systems with constraints because usual shake/rattle procedure is not reversible. The new staging PIMD method does not suffer from this deficiency.

ACKNOWLEDGMENTS

This work was supported by grants from the National Science Foundation CHE-92-22506, B.J.B. and M.E.T.

and CHE-92-23546 (M.L.K. and G.J.M.). One of us (G.J.M.) would like to acknowledge an NSF Postdoctoral Research Associateship in Computational Science and Engineering (ASC-91-08812). We also thank Professor David Coker and Doris Mei for communicating their adaptation of the methods of this paper to Fourier path integrals.

APPENDIX A

Systems undergoing Nosé–Hoover chain dynamics can also be integrated using RESPA. As in the standard Respa method, the operator that generates the dynamics of the system of interest is written as

$$\exp(iL\Delta t) = \exp\left[\Delta F(q) \frac{\partial}{\partial p} \frac{\Delta t}{2}\right] \exp(iL_{\text{hNHC}}\Delta t) \times \exp\left[\Delta F(q) \frac{\partial}{\partial p} \frac{\Delta t}{2}\right] + \mathcal{O}(\Delta t^3), \quad (\text{A1})$$

where $iL = iL_{\text{h+NHC}} + \Delta F(q)(\partial/\partial p)$. Here the reference system is a harmonic oscillator undergoing Nosé–Hoover chain dynamics [see Eqs. (2.24)]. The Nosé–Hoover chains are included in the reference system because for the optimal choice of thermostat mass, $Q = kT/\omega^2$, the thermostat coordinates evolve on the same time scale as the oscillator. As in the text, a further simplification of the reference system propagator can be made

$$e^{iL_{\text{h+NHC}}\Delta t} = \prod_{i=1}^n e^{iL_{\text{h+NHC}}\delta t}, \quad (\text{A2})$$

where $\delta t = \Delta t/n$. The operator $e^{iL_{\text{h+NHC}}\delta t}$ can be applied to an initial state to order $\mathcal{O}(\delta t^3/n^2)$ using a numerical integrator. It remains to specify an integrator for Nosé–Hoover chain dynamics and to show how the operators containing the difference force modify the integrator to form a RESPA scheme.

The Nosé–Hoover chain equations of motion [see Eqs. (2.24)], which are generated by the action of $e^{iL_{\text{h+NHC}}\delta t}$ on an initial state can be integrated using an implicit method based on velocity Verlet.²⁶ The positions are determined by

$$\begin{aligned} q(\delta t) &= q(0) + v_q(0)\delta t + \frac{\delta t^2}{2} \left[\frac{1}{m} F_h(0) - v_{\eta_1}(0)v_q(0) \right], \\ \eta_1(\delta t) &= \eta_1(0) + v_{\eta_1}(0)\delta t + \frac{\delta t^2}{2} \left[\frac{1}{Q} F_{\eta_1}(0) - v_{\eta_2}(0)v_{\eta_1}(0) \right], \\ \eta_2(\delta t) &= \eta_2(0) + v_{\eta_2}(0)\delta t + \frac{\delta t^2}{2} \left[\frac{1}{Q} F_{\eta_2}(0) \right], \end{aligned} \quad (\text{A3})$$

where

$$\begin{aligned} F_h(0) &= -\left. \frac{\partial V_h(q)}{\partial q} \right|_{q(0)}, \\ F_{\eta_1}(0) &= m v_q^2(0) - kT, \\ F_{\eta_2}(0) &= Q v_{\eta_1}^2(0) - kT, \end{aligned} \quad (\text{A4})$$

δt is the time step and the number of thermostats in the chain is set equal to two. The velocities are determined from an iterative procedure

$$v_q^{(i)}(\delta t) = \left\{ v_q(0) + \frac{\delta t}{2} \left[\frac{1}{m} F_h(0) + \frac{1}{m} F_h(\delta t) - v_{\eta_1}(0)v_q(0) \right] \right\} / \left[1 + \frac{\delta t}{2} v_{\eta_1}^{(i-1)}(\delta t) \right],$$

$$v_{\eta_1}^{(i)}(\delta t) = \left\{ v_{\eta_1}(0) + \frac{\delta t}{2} \left[\frac{1}{Q} F_{\eta_1}(0) + \frac{1}{Q} F_{\eta_1}^{(i)}(\delta t) - v_{\eta_1}(0)v_{\eta_2}(0) \right] \right\} / \left[1 + \frac{\delta t}{2} v_{\eta_2}^{(i-1)}(\delta t) \right]$$

$$v_{\eta_2}^{(i)}(\delta t) = v_{\eta_2}(0) + \frac{\delta t}{2} \left[\frac{1}{Q} F_{\eta_2}(0) + \frac{1}{Q} F_{\eta_2}^{(i)}(\delta t) \right] \quad (\text{A5})$$

with initial guess

$$v_{\eta_1}^{(0)}(\delta t) = v_{\eta_1}(-\delta t) + 2\delta t \left[\frac{1}{Q} F_{\eta_1}(0) - v_{\eta_1}(0)v_{\eta_2}(0) \right],$$

$$v_{\eta_2}^{(0)}(\delta t) = v_{\eta_2}(-\delta t) + 2\delta t \left[\frac{1}{Q} F_{\eta_2}(0) \right] \quad (\text{A6})$$

to a desired tolerance. The tolerance is taken to be largest possible value that results in stable integration (too large a tolerance results in a drift in the conserved quantity). This procedure is called implicit velocity Verlet integration.

A RESPA algorithm based on implicit velocity Verlet integration can be constructed. The procedure is designed to reduce to implicit velocity Verlet integration of the full force in the limit that $n=1$ and to the standard RESPA method if the coupling of the oscillator to the Nosé–Hoover chains is eliminated. Again, RESPA breaks up a large time step, Δt , into n small time steps of length, δt . The RESPA method differs from n straightforward applications of implicit velocity Verlet algorithm only on the first and the n th small time steps where the n times the difference force, $n\Delta F$, must be applied. In the first small time step, where the system is advanced from time zero to time δt , the harmonic force, $F_h(0)$, is replaced by the force, $F_h(0) + n\Delta F(0)$, in Eqs. (A3)–(A6). The integration procedure is otherwise unchanged. In the n th small time step, where the system is advanced from time $\Delta - \delta t$ to Δt , the harmonic force, $F_h(\Delta t)$ is simply replaced by the force, $F_h(\Delta t) + n\Delta F(\Delta t)$, in Eqs. (A3)–(A6). Again, the integration procedure is otherwise unchanged. As is the case in the standard velocity Verlet algorithm, the difference force at time Δt is precisely the difference force that must be used in the first step of the next application of the integrator. Therefore, only one difference force evaluation per large time step, Δt , is necessary. In Appendix B, Fortran code for this algorithm is given.

APPENDIX B

Here, some of the fortran code necessary to implement the staging PIMD algorithm is included. Continuation cards have been eliminated for clarity.

```

      SUBROUTINE INTEGRATE
C HERE NP = P OF THE TEXT
C NNOS = M OF THE TEXT
C NRESP = n OF THE TEXT
C DT = Δt OF THE TEXT
C DT1 = Δt OF THE TEXT
C DT1 = Δt OF THE TEXT
C INITIALLY FXUHARM(I) = FXUHARM(I)
C + DBLE(NRESP)*FXUEXT(I) I = 1,NP
C
C THE RESPA LOOP
RN = DBLE(NRESP)
DT1 = DT/RN
DT12 = DT1/2.D0
TDT1 = 2.D0*DT1
DT122 = DT1*DT1/2.D0
DO 10 IRESP = 1,NRESP
C INTEGRATE THE BEAD POSITIONS
DO I = 1,NP
  XU(I) = XU(I) + DT1*VXU(I)
  + DT122*(FXUHARM(I)-VXU(I)*VXULOGS(I,1))
ENDDO
C INTEGRATE THE NOSE-HOOVER VARIABLES
DO I = 1,NNOS*NP
  XULOGS(I,1) = XULOGS(I,1) + DT1*VXULOGS(I,1)
  + DT122*FXULOGS(I,1)
ENDDO
C INTEGRATE THE VELOCITIES A HALF TIME STEP
DO I = 1,NP
  VXUT(I) = VXU(I)
  + DT12*(FXUHARM(I)-VXU(I)*VXULOGS(I,1))
ENDDO
DO I = 1,NNOS*NP
  VXUTLOGS(I,1) = VXULOGS(I,1)
ENDDO
DO I = 1,NNOS*NP
  VXULOGS(I,1) = VXUOLOGS(I,1) + TDT1*FXULOGS(I,1)
ENDDO
DO I = 1,NNOS*NP
  VXUOLOGS(I,1) = 1.0D0/DBLE(I+1)
ENDDO
DO I = 1,NNOS*NP
  VXUTLOGS(I,1) = VXUTLOGS(I,1) + DT12*FXULOGS(I,1)
ENDDO
C GET THE FORCES AT THE NEW POSITIONS
CALL GETFXUHARM
IF(IRESP.EQ.NRESP)THEN
  CALL GETX
  CALL GETFXEXT
  CALL GETFXUEXT
  DO I = 1,NP
    FXUHARM(I) = FXUHARM(I) + RN*FXUEXT(I)
  ENDDO
ENDIF
C ADD THESE FORCES TO THE VELOCITIES
DO I = 1,NP
  VXUT(I) = VXUT(I) + DT12*FXUHARM(I)
ENDDO
C ITERATE THE VELOCITIES TO COVERAGE
5  CONTINUE
DO I = 1,NP
  VXUN(I) = VXUT(I)/(1.D0 + DT12*VXULOGS(I,1))
ENDDO
DO J = 1,NNOS-1
  CALL GETFXULOGS(J)
DO I = 1,NP
  VXUNLOGS(I,J) = (VXUTLOGS(I,J) + DT12*FXULOGS(I,J))
  /(1.D0+DT12*VXULOGS(I,J+1))
ENDDO
ENDDO
CALL GETFXULOGS(NNOS)
DO I = 1,NP
  VXUNLOGS(I,NNOS) = VXUTLOGS(I,NNOS) + DT12*FXULOGS(I,NNOS)
ENDDO
CALL GETTOLNOW
DO I = 1,NP
  VXU(I) = VXUN(I)
ENDDO
DO I = 1,NNOS*NP
  VXULOGS(I,1) = VXUNLOGS(I,1)
ENDDO
IF(TOLNOW.LT.TOL)GOTO 5
DO J = 1,NNOS-1
  DO I = 1,NP
    FXULOGS(I,J) = FXULOGS(I,J) - VXULOGS(I,J)*VXULOGS(I,J+1)
  ENDDO
ENDDO
CONTINUE
SUBROUTINE GETX
C TRANSFORM POSITIONS FROM XU TO X
C HERE NSEG = N OF THE TEXT
C AND NSTAGE+1 = j OF THE TEXT
C
C SET UP SOME USEFUL CONSTANTS
DO I = 1,NSTAGE
  RAT1(I) = DBLE(I)/DBLE(I+1)
  RAT2(I) = 1.0D0/DBLE(I+1)
ENDDO
CONST = DBLE(NSTAGE)/DBLE(NSTAGE+1)
CONST2 = 1.0D0/DBLE(NSTAGE+1)
DO K = 1,NSEG
  III(K) = (K-1)*(NSTAGE+1) + 1
  JJJ(K) = III(K) + (NSTAGE+1)
ENDDO
JJJ(NSEG) = 1
C TRANSFORM THE POSITIONS
DO I = 1,NP
  X(I) = XU(I)
ENDDO
DO K = 1,NSEG
  X(NSTAGE+III(K)) = X(NSTAGE+III(K))
  + CONST*XU(JJJ(K))+XU(III(K))*CONST2
  DO I=NSTAGE-1,1,-1
    X(I+III(K)) = RAT1(I)*X(I+III(K)+1)
    +XU(III(K))*RAT2(I)+ X(I+III(K))
  ENDDO
ENDDO
SUBROUTINE GETFXUEXT
C TRANSFORM FORCES FROM FXEXT TO FXUEXT
C
C SET UP SOME USEFUL CONSTANTS
DO I = 1,NSTAGE
  RAT3(I) = DBLE(I-1)/DBLE(I)
ENDDO
CONST = DBLE(NSTAGE)/DBLE(NSTAGE+1)
DO K = 1,NSEG
  III(K) = (K-1)*(NSTAGE+1) + 1
  JJJ(K) = K*(NSTAGE+1)
  KKK(K) = III(K) - 1
ENDDO
KKK(1) = NP
C TRANSFORM THE FORCES
DO I = 1,NP
  FXUEXT(I) = FXEXT(I)
ENDDO
C THE STAGING BEADS
DO K = 1,NSEG
  DO I=2,NSTAGE
    FXUEXT(I+III(K)) = RAT3(I)*FXUEXT(I+III(K)-1)
    + FXUEXT(I+III(K))
  ENDDO
ENDDO
C THE END POINT BEADS
DO K = 1,NSEG
  FXUEXT(III(K)) = FXUEXT(III(K))
  - CONST*(FXUEXT(JJJ(K))-FXUEXT(KKK(K)))
  + DSUM(NSTAGE,FXEXT(III(K)+1),1)
ENDDO
DO I=1,NP
  FXUEXT(I) = FXUEXT(I)/MASS(I)
ENDDO

```

APPENDIX C

The results of the Sec. IV indicate that MD and HMC can be less efficient than ordinary MC in sampling solvent degrees of freedom. The behavior of HMC is particularly poor. This is may be due to the complete resampling of all

the particle velocities that occurs when a move is rejected. A complete resampling causes the velocities to become uncorrelated, and hence, if one were to measure the velocity autocorrelation function, one would find that it had a short decay time. Since the diffusion coefficient is proportional to this decay time, it will therefore be substantially decreased

by this resampling scheme, a fact which leads the mean square displacements presented in Figs. 7 and 8. Therefore, in the spirit of Andersen,¹⁸ it may be more efficient to resample some fraction of the velocities, γ and maximize the mean square displacement with respect to this parameter. This would make the rejection step a less stochastic event and lead to better diffusion. The same result could perhaps be achieved if several time steps are made before a move is either accepted or rejected. However, the number of time steps selected must be less than the correlation time or the algorithm will be inefficient.

MD is less efficient than MC in very high temperature helium ($T^*=30.23$). At such temperatures, the particles behave like "hard spheres." Collisions are extremely strong, even impulsive, at this temperature and density. Therefore, it is very difficult to integrate through the collisions continuously. This behavior could be improved by using the long range forces version of RESPA⁷ to accurately integrate the collisions. (This would also help HMC.) Nevertheless, even under very extreme conditions, MD still performs adequately. It is 1.6 times less efficient than ordinary MC under these conditions.

The efficiencies discussed above are based on the relative size of the single particle diffusion coefficient. While this is probably adequate for monatomic fluids, it is not, in general, the best measure. A better measure might be the diffusion coefficient in pair space or the decay of the energy autocorrelation function of each particle as this quantity serves as a true test of how well energy is equipartitioning.³² However, the energy measure would clearly fail for a hard spheres system which helium at $T^*=30.23$ begins to approximate. Mountain and Thirumalai have suggested more sophisticated measures of convergence in numerical simulation.³³

- ¹B. J. Berne and D. Thirumalai, *Ann. Rev. Phys.* **37**, 401 (1986).
- ²E. L. Pollock and D. M. Ceperley, *Phys. Rev. B* **30**, 2555 (1984).
- ³M. Parrinello and A. Rahman, *J. Chem. Phys.* **80**, 860 (1984).
- ⁴D. Chandler and P. G. Wolynes, *J. Chem. Phys.* **74**, 4078 (1981).
- ⁵A. J. Lichtenberg and M. A. Lieberman, *Regular and Stochastic Motion* (Springer, New York, 1983).
- ⁶R. W. Hall and B. J. Berne, *J. Chem. Phys.* **81**, 3641 (1984).
- ⁷M. Tuckerman, G. J. Martyna, and B. J. Berne, *J. Chem. Phys.* **97**, 1990 (1992).
- ⁸M. Sprik, M. Klein, and D. Chandler, *J. Chem. Phys.* **83**, 3942 (1985).
- ⁹R. D. Coalson, *J. Chem. Phys.* **85**, 926 (1986).
- ¹⁰J. Doll and D. Freeman, *J. Chem. Phys.* **80**, 239 (1984).
- ¹¹D. Mei and D. F. Coker (private communication, 1993).
- ¹²G. J. Martyna, M. Tuckerman, and M. L. Klein, *J. Chem. Phys.* **98**, 1990 (1992).
- ¹³S. Nosé, *J. Chem. Phys.* **81**, 511 (1984).
- ¹⁴W. G. Hoover, *Phys. Rev. A* **31**, 1695 (1985).
- ¹⁵S. Duane, A. D. Kennedy, B. J. Pendleton, and D. Roweth, *Phys. Lett. B* **195**, 216 (1987).
- ¹⁶S. Duane and J. B. Kogut, *Nucl. Phys. B* **275**, 398 (1986).
- ¹⁷P. G. Bergmann and J. L. Lebowitz, *Phys. Rev.* **99**, 578 (1955).
- ¹⁸H. C. Andersen, *J. Chem. Phys.* **72**, 2384 (1980).
- ¹⁹M. P. Allen and D. J. Tildesley, *Computer Simulations of Liquids* (Clarendon, Oxford, 1989).
- ²⁰R. P. Feynman, *Statistical Mechanics* (Benjamin, Reading, 1972).
- ²¹L. D. Fosdick and H. F. Jordan, *Phys. Rev.* **143**, 58 (1966).
- ²²J. A. Barker, *J. Chem. Phys.* **70**, 2914 (1978).
- ²³M. Herman, E. F. Bruskin, and B. J. Berne, *J. Chem. Phys.* **76**, 1347 (1982).
- ²⁴M. Sprik, M. Klein, and D. Chandler, *Phys. Rev. B* **31**, 4234 (1985).
- ²⁵S. Nosé, *Prog. Theor. Phys. Supp.* **103**, 1 (1991).
- ²⁶W. C. Swope, H. C. Andersen, P. H. Berens, and K. R. Wilson, *J. Chem. Phys.* **76**, 637 (1982).
- ²⁷D. F. Coker, D. Thirumali, and B. J. Berne, *J. Chem. Phys.* **86**, 5689 (1987).
- ²⁸N. Metropolis, A. W. Rosenbluth, M. N. Rosenbluth, A. H. Teller, and E. Teller, *J. Chem. Phys.* **21**, 1087 (1953).
- ²⁹D. Chandler, Y. Singh, and D. M. Richardson, *J. Chem. Phys.* **81**, 1975 (1984).
- ³⁰J. Cao and B. J. Berne, *J. Chem. Phys.* **91**, 6359 (1989).
- ³¹Here σ denotes the relative error in the mean and is equivalent to the quantity Δ in Eq. (2.2) and *not* σ in Eq. (2.1) from Ref. 30.
- ³²M. Rao, C. Pangali, and B. J. Berne, *Mol. Phys.* **37**, 1773 (1979).
- ³³R. D. Mountain and D. Thirumalai, *Comp. Phys. Commun.* **62**, 352 (1991).